Deconvolution of dynamic dual photon microscopy images of cerebral microvasculature to assess the hemodynamic status of the brain

Hatef Mehrabian *[a,b], Liis Lindvere [a,b], Bojana Stefanovic [a,b] and Anne L. Martel [a,b]
[a] Department of Medical Biophysics, University of Toronto, Toronto, ON, Canada
[b] Imaging Research, Sunnybrook Health Sciences Centre, Toronto, ON, Canada

ABSTRACT

Assessing the hemodynamic status of the brain and its variations in various situations are required to understand the local cerebral circulatory mechanisms. Dynamic contrast enhanced imaging of cerebral microvasculature provides information that can be used in understanding physiology of cerebral diseases. Bolus tracking is a technique that can be used to extract characteristic parameters that quantify local cerebral blood flow. However, post-processing of the data is needed to segment the FOV and to perform Deconvolution to remove the effects of input bolus profile and the path it travels to reach the imaging window. Finding the arterial input function (AIF) and dealing with the ill-posedness of deconvolution system make this process difficult. We propose using ICA to segment the FOV and to extract a local AIF as well as the venous output function that is required for deconvolution. This also helps to stabilize the system as ICA suppresses noise efficiently. Tikhoniv regularization (with L-curve analysis to find the best regularization parameter) is used to make the system stable and solve the problem. We have acquired dynamic 2PLSM images of a rat brain in two conditions (when the animal is at rest and when it is stimulated) and performed deconvolution. The experimental along with the simulation studies provided promising results that demonstrate the feasibility and importance of performing deconvolution.

Keywords- Deconvolution, Independent Component Analysis, Two Photon Laser Scanning Microscopy (2PLSM), bolus tracking, Tikhonov regularization, L-curve analysis.

1. INTRODUCTION

Most non-invasive human brain imaging methodologies such as fMRI, PET and near infrared spectroscopy rely on the tight coupling between focal cerebral hemodynamics and neuronal activity [1]. A detailed understanding of the local cerebral circulatory regulation mechanism is critical for establishment of accuracy and range of the applicability of these techniques. CBF (cerebral blood flow) undergoes local (in addition to global) regulation so that on a sub-millimeter scale, maps of hemodynamic changes closely follow those of neuronal activity under a variety of conditions [2],[3]. Many studies have suggested that amplitude and temporal evolution of blood flow response to functional activation follow the cortical neuronal architecture [2],[4]. Increasing evidence has shown that dynamic information derived from dynamic contrast enhanced (DCE) imaging data can be used in understanding the pathophysiology of cerebral diseases [5], [6]. In DCE imaging the contrast agent is injected intravenously and the vascular system is imaged repeatedly over time so as to track the passage of the contrast agent through the vascular bed [7]. The tracer concentration change over time is used to assess the hemodynamic status of the brain [8].

The cerebral vascular system, like the neuronal network, exhibits both hierarchy and spatial specialization. Fenstermacher *et al*. [9] showed that at rest, the blood flow varies up to 18-fold at different regions of a rat brain. This might result from regional differences in capillary density [10]. It can also be caused due to transit time variations in the vasculature [11]. Microcirculatory CBF control is of most interest to brain function investigations due to the proximity of the capillary network to the activated parenchyma. Thus it is crucial to understand how red blood cell (RBC) velocities are regulated [12]. A variety of central nervous system (CNS) conditions, such as stroke, dementia and epilepsy, involve a compromise in the resting blood flow. It is necessary to characterize the spatial pattern of cerebral microvascular network reactivity under physiological conditions.

Although heterogeneous profile of microcirculatory adjustments has long been suspected [13], limited data is available on the reactivity of deep cerebral microvessels, data on spatial pattern of microvascular flow regulation in the brain has been scarce and reported microvessel behavior has been highly variable, likely due to the intrinsic

Medical Imaging 2011: Biomedical Applications in Molecular, Structural, and Functional Imaging,
edited by John B. Weaver, Robert C. Molthen, Proc. of SPIE Vol. 7965, 79650A · ©
2011 SPIE · CCC code: 0277-786X/11/$18 · doi: 10.1117/12.878741

difficulty in achieving the required spatial resolution *in-vivo*. Scanning confocal microscopy enables imaging of individual microvessels below the cortical surface. This has been used to investigate CBF increases elicited by hypercapnia [12],[14]. Two-photon laser scanning microscopy (2PLSM) provides additional important advantages particularly for *in-vivo* biological applications [15]. Recently, the applicability of 2PLSM to investigation of cerebral microcirculation has been shown in rat dorsal olfactory bulb during odor stimulation [16], rat somatosensory cortex [12], etc.

Bolus tracking in 2PLSM is carried out using DCE imaging of the brain to track the passage of a rapidly injected (intravenously) bolus of fluorescent dye (Dextran) through the cerebral microvasculature. By kinetic analysis of these data which involves characterization of passage of the bolus from an artery to the vein or veins that are being fed by that artery, the hemodynamic status of that region of the brain can be inferred. Contrast agent concentration in each vessel changes with hemodynamic status of the brain as well as the variations in the input bolus profile and the path it travels to reach the brain. Thus, the contrast concentration in each voxel is affected by the input bolus which makes it difficult to compare different hemodynamic states of the brain. Therefore, it is necessary to eliminate this effect such that contrast concentration profile of each voxel reflects its hemodynamic status only. This can be done through a process called deconvolution. The goal of this study is to optimize the performance of deconvolution using both simulation and experimental data. The two major issues in deconvolution that are finding the arterial input function (AIF) and handling the ill-posedness of the deconvolution system are addressed here.

2. THEORY AND METHODS

2.1 Convolution model of the cerebral circulation

Assuming a bolus of non-diffusible dye is given to the artery, the individual particles of the bolus follow different paths through the cerebral microvasculature to reach the output vein and their transit times thus have a distribution characteristic of the flow and the vascular structure [17]. The probability density function of these transit times is denoted as $h(t)$, the transport function. Assuming the hemodynamic status of the brain remains unchanged as the bolus passes through the vascular network, the passage mechanism can be considered as a LTI (linear time invariant) system. Thus; when an arterial input $AIF(t)$ is given as the input, the concentration of the bolus in the venous output, $C_v(t)$, is the convolution of the transport function, $h(t)$, (impulse response of the system) with the arterial input function:

$$C_v(t) = h(t) * AIF(t) = \int_0^t h(\tau)AIF(t-\tau)d\tau \quad (1)$$

To assess the changes in hemodynamic status of the brain as its neuronal activity changes, it is necessary to find the transport function of the brain. The effects of neuronal activity in the brain can be assessed by comparing different hemodynamic indices such as mean transit time (MTT) from an artery to a vein, vessel diameter, CBF or CBV in different hemodynamic states.

An ideal bolus would be the one that 1) has a Dirac delta profile and 2) is injected into the feeding artery. In the presence of such a bolus the venous output could be used as the transport function. Neither of these conditions is satisfied in practice. The profile of the injected bolus depends on the duration of injection as well as the amount of dye that is being injected. The injection site is usually far from the feeding artery (usually outside of the brain) and therefore it spreads depending on the path that it travels to reach the feeding artery. Thus, it is necessary to eliminate the effects of the variation in these factors in the venous output or in other word to extract the transport function for the bolus passage from the artery to the vein.

2.2 Methods of performing deconvolution

Two approaches can be taken to solve equation-1 and extract the transport function, 1) the Fourier transform approach and 2) the algebraic approach. In the Fourier transform approach the convolution in equation-1 is converted to a multiplication. This technique is very sensitive to noise and can only be applied at high SNR to find the transport functions with long MTTs [17]. We will therefore use the algebraic approach which is based on

a reformulation of the convolution integral in matrix form as a linear system of equations. It has been used extensively in the analysis of tracer transport analyses [18], [19]. This method assumes the arterial and cerebral concentrations are measured at a set of equally spaced time intervals, $t_1, t_2, \ldots, t_N$, and that over the small intervals the transport function and the AIF are constant. Thus, the convolution in equation-1 can be reformulated as:

$$\begin{bmatrix} C_v(t_1) \\ C_v(t_2) \\ . \\ . \\ . \\ C_v(t_N) \end{bmatrix} = \begin{bmatrix} AIF(t_1) & 0 & . \ . \ . & 0 \\ AIF(t_2) & AIF(t_1) & . \ . \ . & 0 \\ . & . & . & . \\ . & . & . & . \\ . & . & . & . \\ AIF(t_N) & AIF(t_{N-1}) & . \ . \ . & AIF(t_1) \end{bmatrix} \cdot \begin{bmatrix} h(t_1) \\ h(t_2) \\ . \\ . \\ . \\ h(t_N) \end{bmatrix} \tag{2}$$

This system is solved in a least squares manner and as it is usually ill-posed, regularization is required. We used Tikhonov regularization to tackle the ill-posedness of the system. If we rewrite equation-2 as $C_v = Ah$, the linear least squares solution is known as the h that minimizes the residual $\|C_v - Ah\|^2$, where $\|\cdot\|$ is the Euclidean norm. In the deconvolution system the matrix A is usually ill-posed. In order to give preference to a particular solution with desirable properties a regularization term is added to the minimization cost function

$$\min_h \{\|C_v - Ah\|^2 + \lambda^2 \|\Gamma h\|^2\} \tag{3}$$

where Γ is the Tikhonov matrix and λ is a scalar parameter known as the regularization parameter. If preference is given to solutions with smaller norms, the identity matrix can be used as the Tikhonov regularization matrix ($\Gamma = I$). An explicit solution to this system, denoted by $\hat{h}$ is given by:

$$\hat{h} = (A^T A + \lambda^2 \Gamma^T \Gamma)^{-1} A^T C_v \tag{4}$$

The L-curve technique is used to find the optimal regularization parameter λ. In equation-3 $\|\Gamma h\|$ is called the semi-norm and $\|Ah - C_v\|$ is the residual norm of the solution [20]. A convenient way to display information about the regularized solution is to plot the semi-norm versus the residual norm for different values of λ. This plot is called the L-curve of the system and the optimal regularization parameter is the one that minimizes both the semi-norm and the residual norm which is the λ of the maximum curvature point on the L-curve.

2.3 Measuring Arterial input function

Quantification of the cerebral blood flow (CBF) by deconvolving equation-1 and extracting a transport function relies on accurate estimation of the AIF and the venous output. In similar applications that require estimation of AIF such as quantification of CBF using dynamic susceptibility contrast MRI, this quantity is commonly estimated from the signal changes in a major artery. However it has been shown that the delay and dispersion between the major artery and the tissue of interest can cause significant errors [21]. In addition, due to the small field of view of 2PLSM and the fact that dynamic data can only be acquired in one plane, it is not practical to measure AIF in a major artery outside of the imaging window simultaneously. Using a local AIF that is in the imaging field of view can minimize the effect of delay and dispersion. However, estimating AIF requires detection and segmentation of the artery in the dynamic images. In addition, since this local signal is being measured in a small vessel it is usually very noisy which, considering the ill-posedness of deconvolution system, will lead to an unstable system.

In 2PLSM images the signal from each voxel can be assumed proportional to the contrast agent concentration in that voxel. The high resolution of this imaging modality enables fast imaging of small vessels whose diameters are in the order of a few micrometers. Each frame can be considered as the superposition of the signal that is generated in its vessels. Mehrabian *et al.* [22] used ICA to segment the artery, the vein and the capillaries in dynamic 2PLSM images making the assumption that the spatial distribution of different vessels (arteries, veins and capillaries) in the imaging field of are independent of each other. It should be noted that these vessels are not independent in the temporal domain (the signal intensity variations of the vessels are correlated).

Independent component analysis (ICA) is a statistical signal processing approach that aims at extracting underlying features of the data set (unobserved components or source signals) from observed mixtures without assuming any knowledge of the mixing coefficients such that the extracted features are mutually independent

[23]. The core idea of ICA is motivated from blind source separation problem for data model of the form

$$X = AS$$

where $X = [x_1, x_2, \dots, x_N]^T$ is a matrix of the N observed mixtures (frames or images), $S = [s_1, s_2, \dots, s_M]^T$ is a matrix containing the M source signals, independent components or IC's (usually $M \leq N$) and $A \in \mathbb{R}^{N \times M}$ is the mixing matrix. The aim of ICA is to estimate the independent components S and the mixing matrix A having the observed mixture signals X. Classical ICA algorithms try to find an unmixing matrix $W \in \mathbb{R}^{M \times N}$ and estimate the IC matrix $Y = [y_1, y_2, \dots, y_M]^T$ such that

$$Y = WX$$

where rows of Y are statistically independent. The IC's can be recovered up to scaling and permutation.

The goal of this study is to compare the physiological condition in two different states which requires applying ICA to the dynamic 2PLSM images in both cases and estimating their concentration-time curves. However, ICA is a statistical method and therefore the IC images corresponding to the artery or the vein might not be the same if ICA is applied to the two datasets separately and their concentration-time curves cannot be compared. To avoid this, the two datasets (at-rest and stimulated) are concatenated to form a single dataset such that the fist frame of the stimulated state starts after the last frame of the at rest state. ICA is then applied to this new dataset in which the IC images of the artery and the vein are the same for both stimulated and at rest states and therefore their concentration-curves can be compared.

The ICA technique is used to segment the artery and the vein in the FOV [22] and to find their concentration-time curves. Arbitrary scaling is resolved by multiplying each concentration-tine curve by using the IC images as masks to segment the original data X and averaging each segment over time. The ICA results are less noisy and thus suitable for handling ill-posedness of deconvolution.

2.4 Simulation and experimental data

Synthetic data is generated to model the passage of a bolus of dye from an artery to a vein. The dataset contains 100 frames of 64×64 pixels with a temporal resolution of 0.1s. The data is comprised of two components corresponding to the artery and the vein as shown in figure 1a. Gaussian additive noise is added to the data to simulate noisy concentration curves (SNR=1). A gamma variate function or a quadratic function can be used to approximate the transport function (this form for the transport function is chosen based on our observations of the results of deconvolution in various experimental data). We have used arbitrary gamma variate functions as the transport function in our simulation and the concentration-time curve of the artery. The concentration-time curve of the vein is calculated by convolving the artery curve with the transport function (figure 1). Two synthetic datasets are produced to highlight the effects of variation in the input bolus on the resultant venous concentration-time curve. We used the same transport function in both datasets and changed their AIF. Table 1 reports the onset time, time to peak (TTP), full width at half maximum (FWHM) for the AIF and venous output and transit time (the difference between the peaks of the artery and the vein curves) values of the two datasets.

Table 1. Onset time, TTP, full width at half maximum (FWHM) and transit time of the artery and vein of both cases

	Onset time	**Time to peak**	**FWHM**	**Transit time**
Case 1 (artery)	1.5 (s)	1.2 (s)	2 (s)	2 (s)
Case 1 (vein)	2.9 (s)	1.8 (s)	2.2 (s)	
Case 2 (artery)	1.7 (s)	0.7 (s)	1.2 (s)	1.8 (s)
Case 2 (vein)	2.8 (s)	1.4 (s)	1.9 (s)	

2PLSM *in-vivo* images of a rat brain were acquired. An adult male Sprague-Dawley rat was anesthetized with isoflurane, tracheotomized and mechanically ventilated. To enable imaging of the brain, stereotaxic surgery was done to prepare a small (~5mm diameter), closed (1% agarose) cranial window over the forelimb representation in the primary somatosensory cortex (~3.5mm lateral to midline just anterior to bregma). A bolus of the fluorescent contrast agent (Texas Red dextran, 70kDa, 0.05ml, 25mg/kg) was administered through the tail vein. Muscle relaxant was administered to minimize residual motion. 2PLSM was done using a 20x, 0.95NA, 2.0mm working distance objective (Olympus).

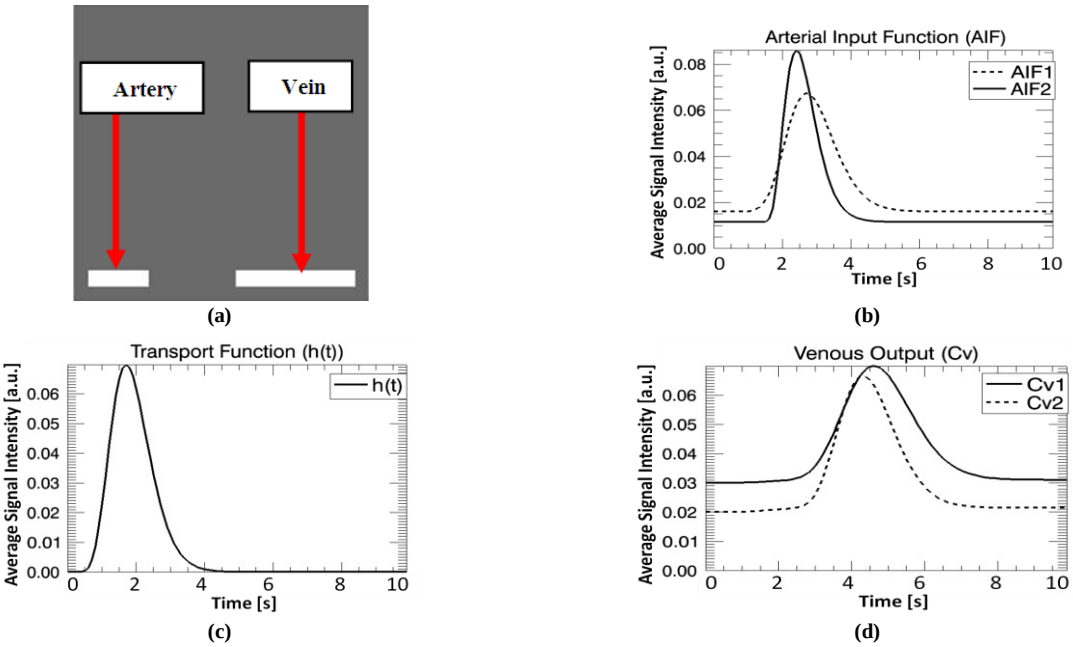

Figure 1 Synthetic data used in simulation study **a)** a sample frame of the datasets, **b)** the AIFs used in the 2 cases, **c)** the transport function, **d)** the venous curves of the two datasets.

The bolus tracking experiments employed a 240^2 matrix over ~450 μm^2 field of view, with a 4 µs dwell time, resulting in a temporal resolution of 0.393s per frame. Imaging was performed in two different hemodynamic states. The first dataset was taken when the animal was at rest and the second set when the animal was stimulated. The imaging FOV was kept the same for both experiments. A sequence of electrical stimulations was applied to the contralateral forelimb. Each pulse was 0.3ms in duration, carrying a current of 2mA, given at a frequency of 3Hz. The stimulation duration was approximately 30s, and the bolus was given at the end of the stimulation.

Figure 2a shows a 3D view of the brain vascular network that was imaged. The imaging was performed in 100µm depth from the surface of the cortex. The network is shown such that the artery and the vein that are used in the study can be seen. Figure 2b shows a sample frame of the first data set in which artery, vein and some capillaries are visible. In this figure the artery and vein appear to be connected, but the static 3-D images of the whole animal brain that was taken at the same time show that these are in fact two vessels aligned in different directions.

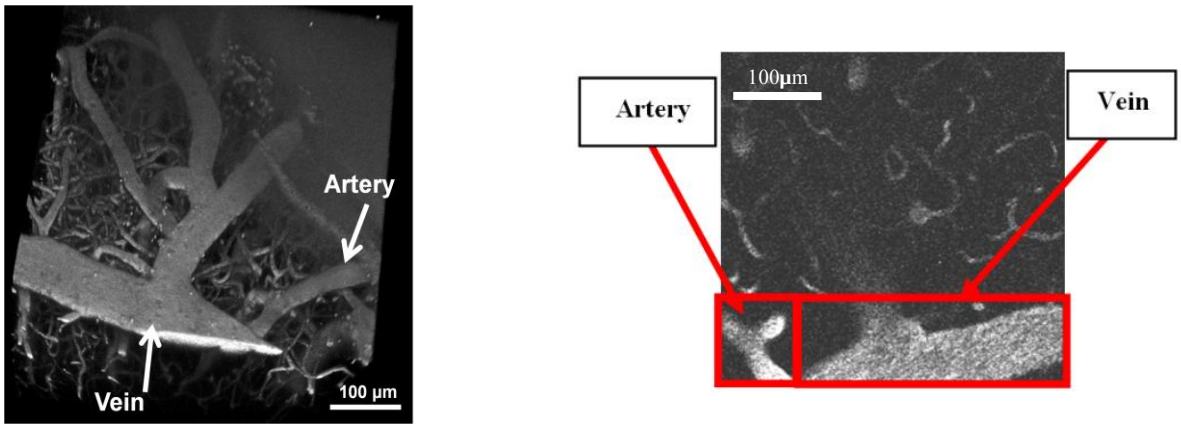

(a) **(b)**

Figure 2 a) 3D view of the vascular network of the rat brain, the network is shown such that the artery and the vein that are used in the study can be seen (the imaging was performed in 100µm depth from the surface of the cortex), **b)** a sample frame of the bolus tracking 2PLSM data in which artery, vein and capillaries are visible

3. RESULTS

3.1 Segmentation

ICA was first applied to each synthetic dataset to separate the artery and the vein. The concentration-time curve that corresponds to the artery is used as the AIF. The segmented artery (or vein) and its corresponding concentration-time curve as well as the original AIF (or venous output) curves for both datasets are shown in figure 3. Although the use of ICA results in significant noise suppression, the system is still ill-posed and regularization is required.

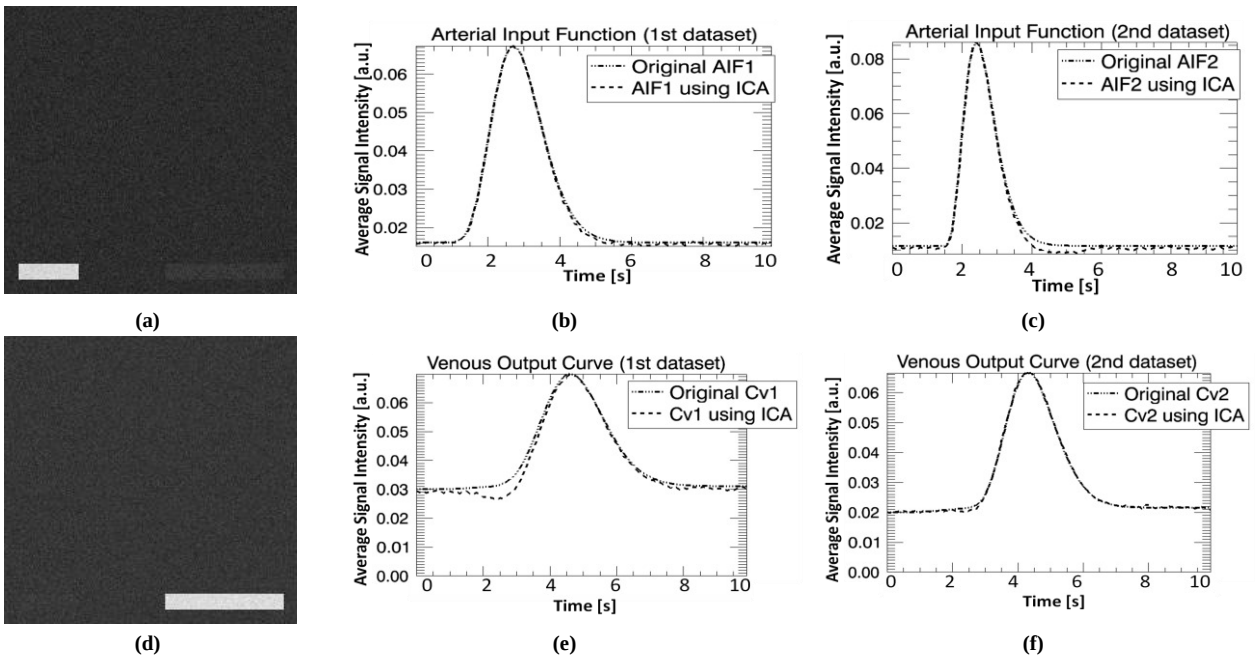

(a) **(b)** **(c)**

(d) **(e)** **(f)**

Figure 3 a) The artery segmented by ICA in both cases. Arterial concentration-time curves for **b)** cases 1, **c)** case 2. **d)** The vein segmented by ICA in both cases. Venous concentration-time curves for **e)** cases1 and **f)** case 2.

A similar process was followed for the two (at rest and stimulated) *in-vivo* rat brain datasets. Here the hemodynamic status is changed in addition to changing the profile of the input bolus. Thus, the shape of the AIF depends on both the input bolus and the hemodynamic status. The results of artery-vein separation using ICA (the artery, the vein and their concentration-time curves) are shown for both datasets in figure 4.

3.2 Deconvolution

Figure 5a shows the original transport function and the transport functions that resulted from the deconvolution of the two synthetic datasets. It can be seen from this figure that although the venous output curves were different, the transport functions resulting from deconvolution are very similar. Table 2 reports the characteristic parameters of the calculated transport functions.

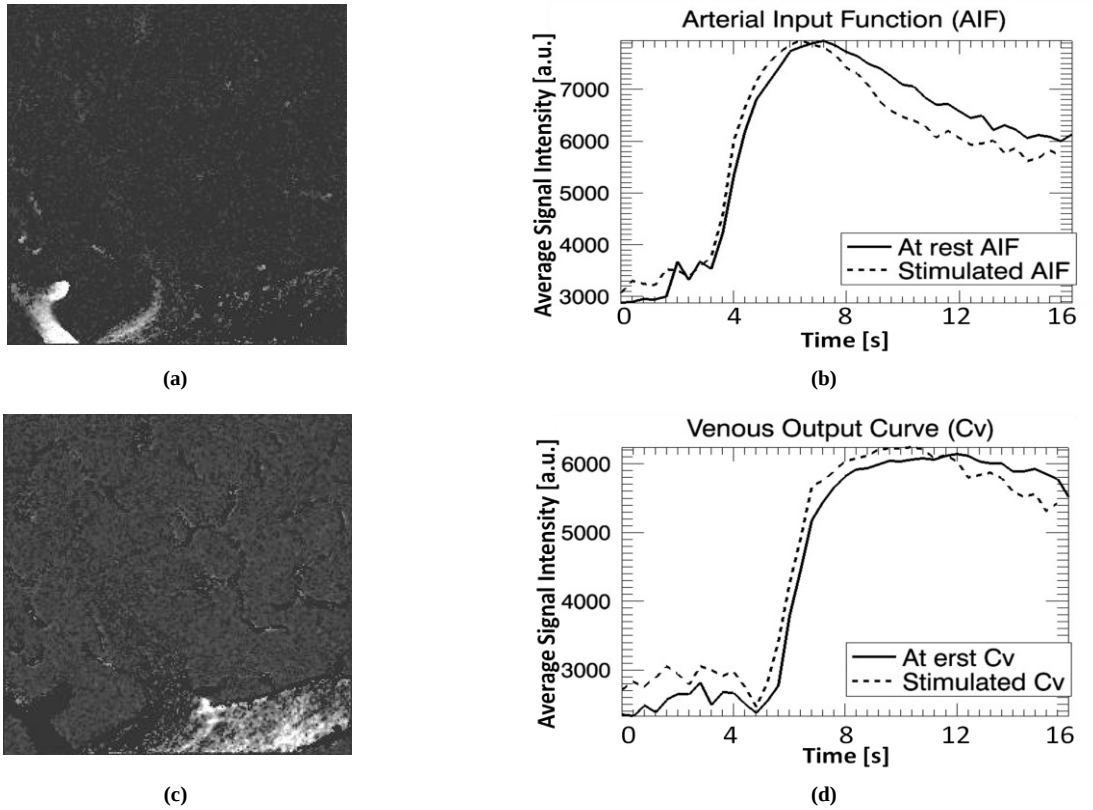

Figure 4. ICA segmentation results, **a, b)** the artery and its corresponding curves in 2 cases, **c, d)** the vein and its corresponding curves in 2 cases

Table 2. Onset time, TTP, FWHM and transit time for the artery and vein of both cases

	Onset time	Time to peak	FWHM	Transit time
Actual	0.7 (s)	1 (s)	1.3 (s)	1.7 (s)
Case 1	0.7 (s)	0.9 (s)	1.4 (s)	1.6 (s)
Case 2	0.6 (s)	1.1 (s)	1.3 (s)	1.7 (s)

In case of the *in-vivo* study, the artery is detected based on the fact that onset time of artery is shorter than the vein. Deconvolution is performed for the two datasets and the resulting transport functions are shown in

figure 5b. It can be seen in this figure the two functions have similar shape and blood moves faster in stimulated case.

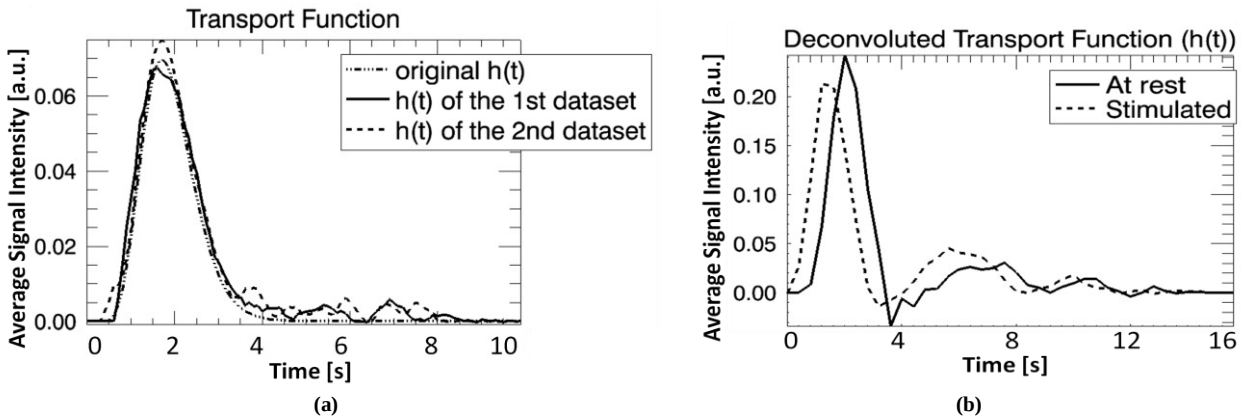

Figure 5. The deconvolved transport functions in both cases for the **a)** simulation study, **b)** experimental study

To characterize the hemodynamic status in the two states, quantitative parameters such as time to peak (TTP), onset time, FWHM and transit time values of the bolus as it travels from the artery to the vein are measured. These parameters are reported for the ICA results before deconvolution in table 3 (the FWHM could not be measured) and after deconvolution in table 4.

Table 3. Onset time, TTP, FWHM and transit time for the artery and vein in both cases

	Onset time	**Time to peak**	**FWHM**	**Transit time**
AIF (At rest)	3.183 (s)	3.93 (s)	N/A	4.716 (s)
Cv (At rest)	5.541 (s)	6.288 (s)	N/A	
AIF (Stimulated)	2.908 (s)	3.41 (s)	N/A	3.930 (s)
Cv (Stimulated)	5.187 (s)	5.069 (s)	N/A	

Table 4. Onset time, TTP, FWHM and transit time for the artery and vein in both cases

	Onset time	**Time to peak**	**FWHM**	**Transit time**
At rest	0.7467 (s)	1.218 (s)	1.965 (s)	1.414 (s)
Stimulated	0.275 (s)	0.904 (s)	1.179 (s)	1.375 (s)

4. DISCUSSIONS

A controlled situation is used in the simulation study to prove the necessity of deconvolution. Simulation results show that deconvolution is a key step in extracting parameters that characterize hemodynamic status of the brain. Ignoring this, results in parameters that are highly dependent on the variations in the input bolus. We kept the transport function constant and changed the input bolus profile which led to a difference in the venous output. Having the same transport function implies similar hemodynamic status but as table 1 shows, using the concentration-time curves of the artery and the vein and measuring the difference between their parameters (time to peak, onset time, etc.) does not reflect the actual transport function and these values change significantly when the input bolus changes.

Figure 3 shows that ICA can be used to segment the images and provide a good estimate of the local AIF in the synthetic data. Using this local AIF removes the dependence of the transport function on the path that the bolus travels to reach the FOV. Table 2 as well as figure 5a show that by deconvolution the actual transport function can be extracted and actual characteristic parameters can be achieved.

In the experimental study a more complex situation is analyzed. The hemodynamic status is changed in addition to changing the profile of the input bolus. As a result the shape of the AIF depends on both the input bolus and the hemodynamic status that affects the bolus profile as it passes through the vascular system. Obtaining correct characteristic parameters to understand the effects of stimulation on the hemodynamic status requires elimination of these effects. As shown in figure 4 ICA results in a good segmentation of the FOV into its underlying components. If we use the concentration-time curves of ICA to measure parameters we will get the values reported in table 3. These values are difficult to measure in addition to being affected by the above mentioned phenomena. We were unable to measure FWHM value as the curves do not drop enough after the peak. Moreover, the peak locations on the venous curves are highly affected by noise and as figure 4 shows the curve almost plateaus and makes locating the maximum difficult. Figure 5b on the other hand shows the transport function clearly. It shows the curves in the two cases have similar shape (unlike the venous curves) which makes them easier to compare and characterize. The transport function of the stimulated state shows a rapid rise (time to peak), a shorter onset time and shorter FWHM compared to the at rest state as reported in Table 4.

5. CONCLUSIONS

Dynamic information derived from DCE images of the cerebral microvasculature can be used to understand the hemodynamic status of the brain and the physiologic condition of cerebral diseases. 2PLSM enables high resolution dynamic imaging of the cerebral vasculature. Bolus tracking can be used to measure characteristic parameters of the cerebral blood flow by monitoring the passage of the bolus through the vascular system from an artery to a vein. Removing the effects of the variations in the input bolus as well as the path that it travels to reach the imaging FOV is essential in measuring these parameters. The convolution model of the cerebral blood flow states that the venous output concentration curve is the convolution of the arterial input function with the transport function. Thus; deconvolution is required to extract the actual transport function and remove the above mentioned effects on the measured parameters.

There are two major problems in performing deconvolution, 1) finding the arterial input function and the venous output; and 2) dealing with the ill-posedness of the deconvolution system. The AIF and venous output are extracted using independent component analysis. ICA is capable of handling noise efficiently which helps in stabilizing the system. Although ICA helps to make the system more stable, regularization is still needed to perform deconvolution. Tikhonov regularization is used here and L-curve analysis is performed to find the optimal regularization parameter. Simulation as well as *in-vivo* experimental studies were performed to show the requirement of the deconvolution and its effect on 2PLSM data. Promising results were achieved showing deconvolution is feasible using the proposed methods and is required to extract accurate parameters characterizing cerebral perfusion.

REFERENCES

[1] Raichle, M. E. “Functional brain imaging and human brain function”, Journal of *Neuroscience*, **23**(10), 3959-3962 (2003).

[2] Cox, S. B., Woolsey, T. A., and Rovainen, C. M. “Localized dynamic changes in cortical blood flow with whisker stimulation corresponds to matched vascular and neuronal architecture of rat barrels” *Journal of Cerebral Blood Flow and Metabolism*, **13**(6), 899-913 (1993).

[3] Logothetis, N. K. “The neural basis of the blood-oxygen-level-dependent functional magnetic resonance imaging signal” *Philosophical Transactions of the Royal Society B: Biological Sciences*, **357**(1424), 1003-1037 (2002).

[4] Lu, H., Patel, S., Luo, F., Li, S., Hillard, C. J., Ward, B. D., *et al*. “Spatial correlations of laminar BOLD and CBV responses to rat whisker stimulation with neuronal activity localized by fos expression” *Mag. Reson. in Med.*, **52**(5), 1060-1068 (2004).

[5] Calamante, F., Gadian, D.G, Connelly, A., “Delay and Dispersion Effects in Dynamic Susceptibility Contrast MRI: Simulations Using Singular Value Decomposition”, *Magn. Reson. Med.*, **44**, pp. 466–473 (2000).

[6] Koenig, M., Kraus, M., Theek, C., Klotz, E., Gehlen, W., Heuser, L., "Quantitative Assessment of the Ischemic Brain by Means of Perfusion-Related Parameters Derived from Perfusion CT", *Stroke,* **32**, pp. 431–437 (2001).

[7] Wu, X.Y, Liu, G.R., "Independent Component Analysis of Dynamic Contrast-Enhanced Images: The Number of Components", *Computational Methods, Netherlands: Springer,* pp. 1111-1116 (2006).

[8] Wu, X.Y., Liu, G.R., "Application of Independent Component Analysis to Dynamic Contrast-Enhanced Imaging for Assessment of Cerebral Blood Perfusion", *Med Image Anal*. Jun, **11**(3), 254-65 (2007).

[9] Fenstermacher, J.D, Nakata, H., Tajima, A., Lin, S.Z., Otsuka, T., Acuff, V., Wei, L., Bereczki, D., "Functional Variations in Parenchymal Microvascular Systems within the Brain", *Magn. Reson. Med*. **19**, pp. 217–220 (1991).

[10] Patlak, C.S., Blasberg, R.G., Fenstermacher, J.D., "An Evaluation of Errors in the Determination of Blood Flow by the Indicator Fractionation and Tissue Equilibration (Kety) Methods", *J. Cereb. Blood Flow Metab.*, **4**, pp. 47– 60 (1984).

[11] Rosen, B.R., Belliveau, J.W., Buchbinder, B.R., McKinstry, R.C., Porkka, L.M., Kennedy, D.N, "Contrast Agents and Cerebral Hemodynamics", *Magn. Reson. Med.*, **19**, pp. 285–292 (1991).

[12] Hutchinson, E.B., Stefanovic, B., Koretsky, A.P., and Silva, A.C., "Spatial flow-volume dissociation of the cerebral circulatory response to mild hypercapnia", *NeuroImage,* **32**(2), 520-530 (2006).

[13] Rosenblum, W.I., "Cerebral Microcirculation: A Review Emphasizing the Interrelationship of Local Blood Flow and Neuronal Function", *Angiology,* **16**, 485-507 (1965).

[14] Villringer, A., Them, A., Lindauer, U., Einhäupl, K., and Dirnagl, U., „Capillary perfusion of the rat brain cortex: An *in-vivo* confocal microscopy study", *Circulation research,* **75**(1), 55-62 (1994).

[15] Denk, W., Strickler, J.H., Webb, W.W., "Two-Photon Laser Scanning Fluorescence Microscopy", *Science,* **248**, pp. 73–76 (1990).

[16] Chaigneau, E., Oheim, M., Audinat, E., Charpak, S., "Two-Photon Imaging of Capillary Blood Flow in Olfactory Bulb Glomeruli", *Proc. Natl. Acad. Sci. U.S.A.*, **100**, pp. 13081– 13086 (2003).

[17] Østergaard, L., Weisskoff, R.M., Chesler, D.A., Gyldensted, G., and Rosen, B.R. "High resolution measurement of cerebral blood flow using intravascular tracer bolus passages. part I: Mathematical approach and statistical analysis", *Magnetic Resonance in Medicine,* **36**(5), 715-725 (1996).

[18] Valentinuzzi, M.E, Volachec, E.M.M., "Discrete deconvolution", *Med. Biol. Eng.* **13**, 123-125 (1975).

[19] Van Huffel, S., Vandewalle, J., De Roo, M.C., Willems, J.L., "Reliable and efficient deconvolution technique based on total linear least squares for calculating the renal retention function", *Med. Bid. Eng. Comput.* **25**, 26-33 (1987).

[20] Hansen, P.C., "Analysis of discrete ill-posed problems by means of the L-curve", *Society for Industrial and applied Mathematics, SIAM review,* **34**(4), pp. 561-580 (December 1992).

[21] Calamante, F., Yim, P.J, Cebral, J.R., "Estimation of bolus dispersion effects in perfusion MRI using image-based computational fluid dynamics", *NeuroImage* **19**:341–353 (2003).

[22] Mehrabian, H., Stefanovic, B., Lindvere, L. and Martel, A. L., "A temporally constrained ICA (TCICA) technique for artery-vein separation of cerebral microvasculature", *in Medical Imaging: Biomedical Applications in Molecular, Structural, and Functional Imaging, Proceedings of SPIE 7626* (2010).

[23] Comon, P. "Independent component analysis, A new concept?", *Signal Processing* **36**(3):287-314 (1994).